A&A 419, 335–343 (2004)
DOI: 10.1051/0004-6361:20040070
© ESO 2004

Astronomy & Astrophysics

Wind accretion in binary stars

I. Mass accretion ratio

T. Nagae[1], K. Oka[1], T. Matsuda[1], H. Fujiwara[2], I. Hachisu[3], and H. M. J. Boffin[4,5]

[1] Department of Earth and Planetary Sciences, Kobe University, Rokko-dai 1-1, Nada-ku, Kobe 657-8501, Japan
e-mail: tmatsuda@kobe-u.ac.jp
[2] IBM Japan Ltd., Yamato-shi, Kanagawa 242-8502, Japan
[3] Department of Earth Science and Astronomy, College of Arts and Sciences, University of Tokyo, Komaba 3-8-1, Meguro-ku, Tokyo 153-8902, Japan
e-mail: hachisu@chianti.c.u-tokyo.ac.jp
[4] Royal Observatory of Belgium, Av. Circulaire 3, 1180 Brussels, Belgium
[5] European Southern Observatory, Karl-Schwarzschild-Str. 2, 85738 Garching, Germany

Received 12 April 2002 / Accepted 16 February 2004

Abstract. Three-dimensional hydrodynamic calculations are performed in order to investigate mass transfer in a close binary system, in which one component undergoes mass loss through a wind. The mass ratio is assumed to be unity. The radius of the mass-losing star is taken to be about a quarter of the separation between the two stars. Calculations are performed for gases with a ratio of specific heats $\gamma = 1.01$ and $5/3$. Mass loss is assumed to be thermally driven so that the other parameter is the sound speed of the gas on the mass-losing star.

Here, we focus our attention on two features: flow patterns and mass accretion ratio, which we define as the ratio of the mass accretion rate onto the companion, $\dot{M}_{\rm acc}$, to the mass loss rate from the mass-losing primary star, $\dot{M}_{\rm loss}$. We characterize the flow by the mean normal velocity of the wind on the critical Roche surface of the mass-losing star, $V_{\rm R}$. When $V_{\rm R} < 0.4\ A\Omega$, where A and Ω are the separation between the two stars and the angular orbital frequency of the binary, respectively, we obtain Roche-lobe over-flow (RLOF), while for $V_{\rm R} > 0.7\ A\Omega$ we observe wind accretion. We find very complex flow patterns in between these two extreme cases. We derive an empirical formula of the mass accretion ratio as $0.18 \times 10^{-0.75 V_{\rm R}/A\Omega}$ in the low velocity regime and $0.05\,(V_{\rm R}/A\Omega)^{-4}$ in the high velocity regime.

Key words. accretion, accretion disks – hydrodynamics – stars: binaries: general

1. Introduction

Wind accretion plays an essential role especially in the evolution of detached binary systems such as symbiotic stars, precursor of peculiar red giants, ζ Auriga stars and massive X-ray binaries. In the majority of symbiotic stars, the system contains a hot component – believed to be a mass-gaining white dwarf – and a cool component, the mass-losing red giant (e.g., Mikołajewska 1997 for a review). Recent studies indicate that many of the red giant components in symbiotic stars do not fill their Roche lobe, i.e., $R_{\rm RG} \lesssim \ell_1/2$, where $R_{\rm RG}$ is the radius of the red giant component and ℓ_1 is the distance of the inner Lagrangian point from the centre of the red giant (e.g., Mürset & Schmid 1999). This possibly discloses that symbiotic stars are – with probably only the exception of T CrB (e.g., Anupama & Mikołajewska 1999) – well detached binary systems. Thus, mass transfer in symbiotic stars seems to be driven by wind, and wind mass loss is therefore a key ingredient for triggering symbiotic activity on a white dwarf companion. On the other hand, the mass accretion rates expected in the Bondi-Hoyle picture (Bondi & Hoyle 1944) for such detached binary systems are usually much lower than those required to maintain the symbiotic activity of the systems. For example, Nussbaumer (1991) pointed out that in most symbiotic stars the typical rates of wind mass loss red giant are in the range $1 \times 10^{-6}\ M_\odot\,{\rm yr}^{-1}$ to $1 \times 10^{-8}\ M_\odot\,{\rm yr}^{-1}$ and that the expected accretion efficiency of wind capture is probably no better than one percent. Hence, the accretion rates associated with most symbiotic white dwarfs are probably in the range of $1 \times 10^{-8}\ M_\odot\,{\rm yr}^{-1}$ to $1 \times 10^{-10}\ M_\odot\,{\rm yr}^{-1}$, which are too low to power the typical luminosities of symbiotics ($\gtrsim$1000 $L_\odot$) unless they are all in a late phase of hydrogen shell-flash (novae) on a white dwarf (e.g., Sion & Ready 1992; Sion & Starrfield 1994). It will nevertheless be shown in the present paper that the mass accretion rate is smaller than that expected by a simple Bondi-Hoyle picture.

Send offprint requests to: H. M. J. Boffin,
e-mail: hboffin@eso.org

Article published by EDP Sciences and available at http://www.aanda.org or http://dx.doi.org/10.1051/0004-6361:20040070

It has recently been suggested that some of the mass-accreting white dwarfs in symbiotic stars are the progenitors of type Ia supernovae (e.g., Hachisu & Kato 2001). On the other hand, it has long been discussed that the efficiency, the ratio of the mass captured by the white dwarf to the mass lost by the red giant, is very small (say, a few per cent) and not enough to increase the white dwarf mass to the Chandrasekhar mass limit (e.g., Kenyon et al. 1993).

Wind velocities in cool red giants are typically a few times 10 km s^{-1} and comparable to the orbital velocity in most symbiotic binary systems. Therefore, flow patterns are probably something between Roche lobe overflow (RLOF) and Bondi-Hoyle wind accretion kinds of flows. The efficiency of capture in symbiotics should therefore not be estimated by the Bondi-Hoyle picture but by direct simulations of intermediate, complicated flow patterns.

Symbiotic stars are not the only systems in which wind accretion play a significant role. The most adopted model for the formation of peculiar red giants, barium, CH and S stars, require a binary system containing an Asymptotic Giant Branch star (AGB) transferring mass via its stellar wind to a main sequence companion which becomes polluted in carbon and s-process elements (see e.g. Boffin & Jorissen 1988). The AGB then evolve into a white dwarf while the companion will appear as carbon or s-process rich and, when on the giant branch, as a peculiar red giant. Boffin & Zacs (1994) have shown that an accretion efficiency of only a few percent is enough to explain present Barium stars. Objects related to these are the extrinsic S stars which also show symbiotic activity (e.g. Carquillat et al. 1998) and bipolar planetary nebulae (e.g. Mastrodemos & Morris 1998).

ζ Aurigae systems are another kind of system where wind accretion plays a role. In these eclipsing double-lined binaries, a main sequence star has an accretion wake produced by the wind of its K supergiant companion. The eponymous system, ζ Aur, is a binary with a 972 days orbital period and containing a 5.8 $M_\odot$ K4 Ib and a 4.8 $M_\odot$ B5 V star (Bennett et al. 1996).

Finally, accretion wakes are also reported for high mass X-ray binaries (HMXB). These systems consist of a compact object, neutron star or black hole, orbiting a massive OB primary star which has a strong stellar wind. The X-ray emission is believed to be due to accretion of matter on the compact companion.

There have been already many numerical studies of stellar wind in a close binary system. Biermann (1971) computed two-dimensional stellar wind using a characteristic method. Sorensen et al. (1975) performed two-dimensional finite difference calculation of stellar wind emitted from a Roche lobe filling secondary. They used the Fluid in Cell (FLIC) method with first order of accuracy and a Cartesian grid. They computed Roche lobe overflow (RLOF) as well. Sawada et al. (1984) calculated two-dimensional stellar wind from a contact binary using a Beam-Warming time implicit finite difference scheme and a generalized curvilinear coordinate. Their main goal was to compute the angular momentum loss rate from the system, which is an important factor to define the evolution of the binary system. Sawada et al. (1986) computed two-dimensional stellar wind from a semi-detached binary system using the Osher upwind scheme and a generalized curvilinear coordinate. They observed a transition from RLOF to stellar wind by increasing the wind speed on the mass-losing star. The present study is a three-dimensional version of their study. Matsuda et al. (1987) also conducted a similar study and discovered a flip-flop instability of the bow shock formed around a compact mass accreting object (see also Boffin & Anzer 1994, and on the stability issue, Foglizzo & Ruffert 1997, 1999, and Pogolerov et al. 2000). However, it was found that the phenomenon was characteristic to two-dimensional case (Matsuda et al. 1992; Ruffert 1996). In the present work we perform three-dimensional calculation in which we do not observe the flip-flop instability.

These simulations concerned the case of a compact object moving in a wind and were mostly aimed at estimating the validity of the Bondi-Hoyle accretion rate. Binary effects were partially simulated by including velocity or density gradient in the wind. There are a few simulations however which simulate in full mass transfer by wind in a binary system (Blondin et al. 1991; Theuns & Jorissen 1993; Blondin & Woo 1995; Theuns et al. 1996; Walder 1997; Mastrodemos & Morris 1998; Dumm et al. 2000; Boroson et al. 2001; Gawryszczak et al. 2002). Theuns & Jorissen (1993) and Theuns et al. (1996, TBJ96 in the following) performed three-dimensional hydrodynamic simulations of a 3 $M_\odot$ AGB transferring mass through its stellar wind to a 1.5 $M_\odot$ main sequence companion, in order to test the wind accretion model for the origin of peculiar red giants. They performed simulations using a polytropic equation of state with $\gamma = 1.$, 1.1 and 1.5 and found mass accretion ratios (that is, mass accretion rate/mass loss rate) of 1−2% for the $\gamma = 1.5$ case and 8% for the other models, i.e. about ten times smaller than the theoretical Bondi-Hoyle estimate. They also observed that this value is dependent on resolution.

Walder (1997) presented simulations of wind accretion in well separated binaries for three different cases: a HMXB, ζ Aur and a barium star progenitor. He obtains mass accretion ratio (mass accretion rate/mass loss rate) of 0.6, 3 and 6%, respectively. Walder & Folini (2000) also presented a nice review of wind dynamics in symbiotics binaries, with an emphasis on the influence of the radiation field of the accretor.

More recently, Dumm et al. (2000) presented three-dimensional Eulerian isothermal simulations in order to represent the symbiotic system RW Hya which seems to present an accretion wake, as indicated by the reduced UV flux observed at phase $\Phi = 0.78$. They found that 6% of the M-giant wind is captured by the companion.

In this paper we perform three-dimensional numerical simulations of mass transfer by wind in a binary system with a mass ratio of unity. The full gravitational forces of the two components are taken into account. This is therefore different from the e.g. TBJ96 or Dumm et al. (2000) studies, where in order to account for the not very well known acceleration mechanism of the wind, the gravitational force of the primary is partially or totally reduced.

Here, we will concentrate on the derivation of the mass accretion ratio. We will leave for a following paper the physical discussion of the flow, including a discussion of angular momentum loss from the system.

2. Assumptions and numerical method

2.1. Model

Consider a detached binary system of equal mass: one larger star blows stellar wind which the other, more compact, component partly accretes. We normalize the length by the separation of the two stars, A, and the time by $1/\Omega$, where Ω is the angular velocity of the binary system. The surface of the mass-losing star is assumed to be an equi-potential surface, whose mean radius is 0.25. The radius of the mass accreting star is assumed to be 0.015 or smaller.

From an OB star, stellar wind is mainly accelerated by line absorption of UV radiation. In symbiotic stars or in precursors of peculiar red giants (PPRGs), the stellar wind mechanism from the cool star is poorly known, and may imply radiation onto dust grains. One needs however to still bring the matter far enough away from the star so that dust grains can form. In more evolved red giants, this may be done through the effect of pulsation. It is however still not clear what the mechanism could be in non-pulsating red giants, as they seem to exist in some symbiotic or extrinsic S stars.

It is therefore clear that simplifying assumption have to be made. In the present study, we will thus simply assume that the wind is generated by thermal pressure, like in the solar wind. More complicated wind structures will be studied in a forthcoming paper.

We assume that the gas is an ideal one and is characterized by the ratio of specific heats, γ. In the present work we consider two extreme cases: $\gamma = 5/3$ and $\gamma = 1.01$. In the latter case, the gas is almost isothermal except where there are shocks. This isothermality may be explained as an outcome of good thermal conduction. We neglect other complex effects like magnetic fields, radiation and viscosity (except numerical one).

We have carried out our simulations for the case of a mass ratio unity. Although this may not be representative for PPRGs, symbiotic stars or HMXBs, this should not change very much our results.

2.2. Method of calculation

We solve the three-dimensional Euler equations using a finite volume scheme. As Riemann solver, we use the SFS scheme and we apply the MUSCL method to interpolate physical variables in a cell; the details on the scheme is described in Makita et al. (2000), and RLOF simulations using the same method are given in Fujiwara et al. (2001).

Calculations are done in the rotating frame of a binary and include the gravity of the two stars, the centrifugal and Coriolis forces. We use a Cartesian coordinate with the origin at the mass accreting star. The computational region is $-1.5 < x < 0.5$, $-0.5 < y < 0.5$, $0 < z < 0.5$ and we assume symmetry around the orbital plane (Fig. 1).

The region is divided into $201 \times 101 \times 51$ cells. The mass accreting companion star is represented by a cubic hole with cells of $3 \times 3 \times 3$, including the lower half of the hole under the orbital plane. Its physical dimension is $0.03 \times 0.03 \times 0.03$ in our units.

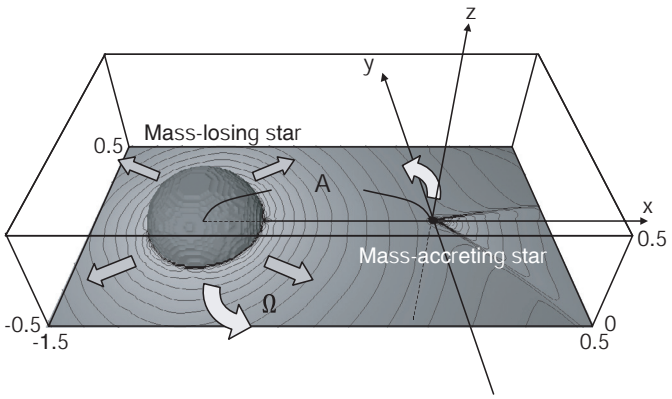

Fig. 1. Computational region.

In order to study in details the structure of the flow near the mass accreting object, we introduce a three levels nested grid. At the second level, the region $-0.25 < x < 0.25$, $-0.25 < y < 0.25$ and $0 < z < 0.25$ is further divided into $102 \times 101 \times 51$ cells. At the third level, the region $-0.125 < x < 0.125$, $-0.125 < y < 0.125$ and $0 < z < 0.125$ is once more divided into $104 \times 104 \times 54$ cells. The cell size of the third level is thus 1/4 of the original first level cell. The hole of $3 \times 3 \times 3$, in the first level, is represented by a hole with $12 \times 12 \times 12$ cells in the third level.

A typical symbiotic star, ζ Auriga or PPRG has an orbital period of a few years and a separation of a few AU. In this case, the cell size of 0.03 is of the order or even larger than a main sequence star. This is thus applicable for ζ Aurigae or PPRGs. For S or symbiotic stars, we should simulate the case of an accreting white dwarf. This would require a hole about 100 times smaller. This is well beyond present days numerical capabilities. This is also true if one would like to simulate the compact accreting object in HMXBs.

One should note however that the size of our accreting object is still smaller than the one adopted by e.g. TBJ96. They have shown that the mass accretion rate decreases with decreasing accreting size and our value is similar to their highest resolution model. We thus also consider a case of a hole having a size of $3 \times 3 \times 3$ cells (i.e. of physical dimensions $\simeq 0.01 \times 0.01 \times 0.01$) at the third level in order to investigate the effect of the size of the mass accreting object on the results.

2.3. Boundary and initial conditions

The outer parts of the mass-losing star is filled by a gas of density $\rho = 1$ and sound speed c_s. If the pressure inside the mass-losing star is larger than that outside the mass-losing star, gas is ejected from the surface. The velocity of the ejected gas is computed by solving a Riemann problem between the two states.

At $t = 0$ the computational region except the mass-losing star is filled by a tenuous gas with density $\rho_0 = 10^{-5}$, velocity $u_0 = v_0 = w_0 = 0$ and pressure $p_0 = 10^{-4}/\gamma$. The computational region is gradually filled with the gas ejected from the mass-losing star. The outside of the computational region is filled by the initial gas all the time. Mass outflow/inflow from the outer boundary can occur; the amount of outflow/inflow

Table 1. Model parameters. The parameters c_s, V_R and f are the sound speed on the surface of the mass losing star, the normal velocity at the critical Roche surface and the mass accretion ratio.

	$\gamma = 5/3$			$\gamma = 1.01$			Nested Grid ($\gamma = 1.01$)		
c_s	Case	V_R	f	Case	V_R	f	Case	V_R	f
0.5		———		a	0.06	1.7×10^{-1}		———	
0.75	B	0.01	3.4×10^{-1}	b	0.46	9.2×10^{-2}	b′	0.46	1.1×10^{-1}
0.9	C	0.03	1.0×10^{-1}	c	1.09	2.4×10^{-2}	c′	1.09	2.2×10^{-2}
1.0	D	0.12	1.9×10^{-2}	d	1.41	1.1×10^{-2}	d′	1.41	1.2×10^{-2}
1.2	E	0.68	3.3×10^{-2}	e	1.95	3.8×10^{-3}	e′	1.94	3.9×10^{-3}
1.4	F	1.49	1.1×10^{-2}	f	2.42	1.6×10^{-3}	f′	2.41	1.8×10^{-3}
1.6	G	1.86	7.4×10^{-3}	g	2.86	6.4×10^{-4}	g′	2.85	5.4×10^{-4}
1.8	H	2.20	3.6×10^{-3}	h	3.29	4.7×10^{-4}		———	
2.0	I	2.52	2.1×10^{-3}	i	3.71	3.6×10^{-4}	i′	3.69	3.3×10^{-4}
2.5	J	3.29	7.9×10^{-4}	j	4.75	2.4×10^{-4}	j′	4.71	2.3×10^{-4}

is also calculated by solving Riemann problems between two states. This (outside) boundary condition, which we call the ambient condition, insures the stability of the computation. The inside of the mass accreting hole is almost vacuum and the gas approaching the hole is absorbed.

We start the calculation at $t = 0$ and terminate it when the system becomes steady. In the wind cases half an orbital period is enough to reach a steady state, but in the RLOF cases we have to calculate at least a few orbital periods.

3. Numerical results

3.1. Parameters

As was described earlier, we adopt γ and the dimensionless sound speed of gas in the mass-losing star, c_s, as the model parameters. In the present work, we consider the cases of $\gamma = 1.01$ and $\gamma = 5/3$. When c_s is less than some critical value, we expect RLOF type flows, while in the other cases, we expect stellar wind kind of flows. As is shown in Table 1, we study the cases of $c_s = 0.5$–2.5 for $\gamma = 1.01$, and $c_s = 0.75$–2.5 for $\gamma = 5/3$.

In PPRGs and symbiotic stars, the sound speed at the surface of the mass-losing giant is of the order of 5–20 kms^{-1} while the orbital velocity is of the order of 10–40 kms^{-1}. In ζ Aurigae, both these values are around 40–100 kms^{-1}, while in HMXBs, the wind speed is of the order of a few thousands of kms^{-1} while the orbital velocity is several hundreds of kms^{-1}.

The parameter c_s has no physical significance, because the mean radius, 0.25, of the mass losing star is chosen arbitrarily for numerical purposes. Using the results of our numerical simulations, we therefore calculate the mean value of the vertical component of the gas speed on the critical Roche surface, V_R. We classify the flow pattern using V_R, which is shown in Table 1 as well. It has to be emphasized that V_R is not constant along the critical Roche surface, especially in the Roche lobe type of flows. For these, it may be better to use c_s as a parameter. For the wind accretion type of flow, which are more isotropic, V_R is more appropriate.

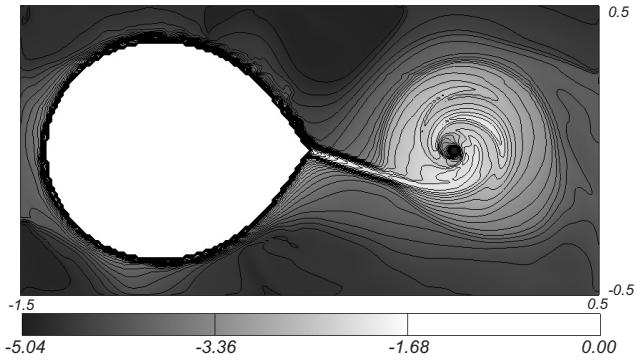

Fig. 2. Density contours in the orbital plane of the typical RLOF case, but in a semi-detached binary system ($\gamma = 1.01$, $c_s = 0.02$).

3.2. Roche lobe overflow

In a typical Roche lobe overflow (RLOF), gas on the surface of the companion flows through the L1 point and forms a narrow L1 stream. The L1 stream deflects its motion to the negative y direction in the present configuration due to the Colioris force, and then circulates counterclockwise around the mass-accreting star to form an accretion disc. We show an example of such typical ROLF flow in the case of $\gamma = 1.01$ in Figs. 2 and 3. Here we assumed the star to fill its Roche lobe, so this is not the main aim of this paper. They will serve as comparison for the B–D and a cases discussed below.

If the temperature of the surface of the companion star, c_s, is raised, the L1 stream becomes thicker (Fujiwara et al. 2001). We define the flow to be of the RLOF type if the flow circulates around the accreting object in counterclockwise direction.

If we raise c_s further, the gas escapes from the mass losing star in all directions, and part of the gas rotates in a clockwise direction around the companion. These two flows, rotating counterclockwise and clockwise, collide behind (i.e. to the right) the accreting object to form a bow shock. This is a typical wind accretion flow.

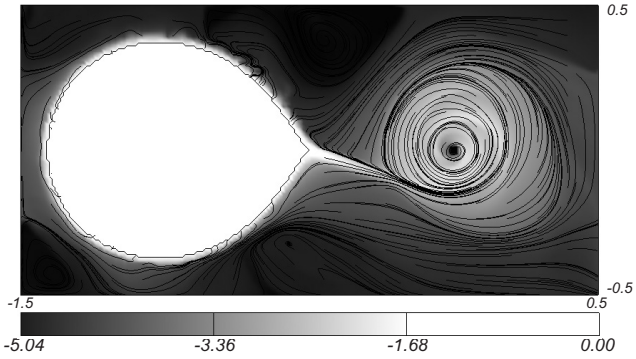

Fig. 3. Streamlines and Mach number counters of the typical RLOF case ($\gamma = 1.01$, $c_s = 0.02$).

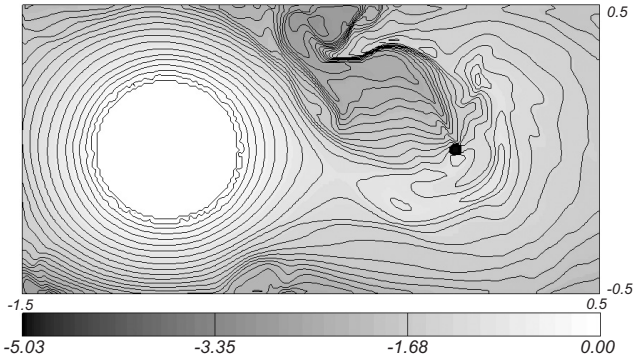

Fig. 4. Density contours in the orbital plane of the RLOF type flow of model B ($\gamma = 5/3$, $V_R = 0.01$). The left circle shows the mass losing companion star with a radius of 0.25, and the right black dot indicates the mass accreting object with a radius of 0.015.

In the B–D cases for $\gamma = 5/3$ and the *a* case for $\gamma = 1.01$, we see from Table 1 that $V_R < 0.4$, i.e. V_R is smaller than the escape velocity. The flow is of the RLOF type. Similar types of flows have been obtained by other authors, e.g. Bisikalo et al. (1998).

Figure 4 shows the density contours for model B ($\gamma = 5/3$, $V_R = 0.01$), and Fig. 5 depicts the streamlines for the same case. In this case, since $\gamma = 5/3$, the temperature of the disc is so hot that the mass accretion ratio f, which is defined in Sect. 3.6, is not 1 but 0.34. Spiral shocks, typical of RLOF flows (Makita et al. 2000; Matsuda et al. 2000; Fujiwara et al. 2001) are not seen in this case.

One should note that contrarily to the impression one might have when just looking at the figures, we have checked that there is no inflow from the outer boundaries in these simulations.

Figure 6 shows the comparison of model a ($\gamma = 1.01$, $V_R = 0.06$) and D ($\gamma = 5/3$, $V_R = 0.12$). We observe spiral shocks, although with a very much distorted shape.

3.3. Intermediate flow

In the cases E, b and b′, we observe that $0.4 < V_R < 0.7$. In these cases, the flow is not a typical RLOF or a wind accretion

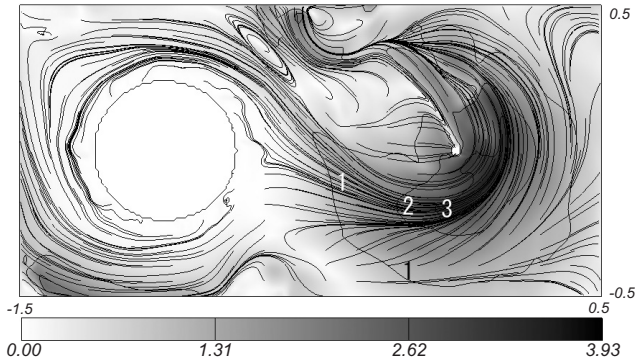

Fig. 5. Streamlines and Mach number contours in the orbital plane of the same model B as in Fig. 2. The Mach number contours are represented by the shade, and the numbers in the figure show typical Mach numbers. Streamlines are generated from points separated by the same distance. We observe that the flow rotates counterclockwise around the companion, which is a typical feature of RLOF type flows.

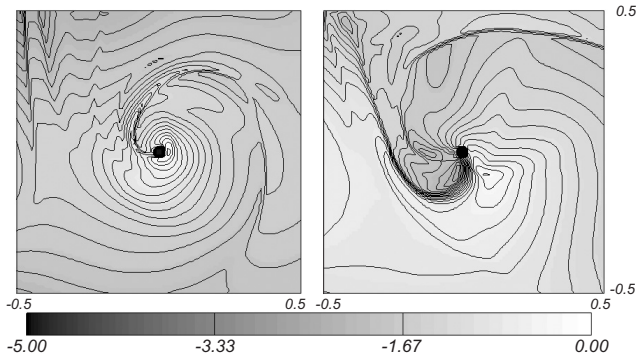

Fig. 6. Comparison of two RLOF type flows. Density contours in the orbital plane are shown. *Left*: model a ($\gamma = 1.01$, $V_R = 0.06$); *right*: model D ($\gamma = 5/3$, $V_R = 0.12$). We observe spiral shocks which are typical to RLOF.

flow, but rather a very complicated intermediate one. Figure 7 shows the density contours of model E, and Fig. 8 depicts the streamlines of the same model.

Figure 9 shows the density contours and the streamlines of the case b. We find that the flow pattern and the shock structure are very complicated in these intermediate flow.

We will now speculate on the possible cause of the complicated structure of the intermediate flow. Gas flows from the mass-losing star (left sphere) towards the mass accreting object (right small sphere). The lower part of the flow experiences a shock, and is decelerated to subsonic speed. A small accretion disc is formed around the companion, but some part of the gas is accelerated to supersonic velocity again. It collides with the gas coming from the positive y side and forms a bow shock. The orientation of the bow shock is rotated almost 90 degrees counterclockwise.

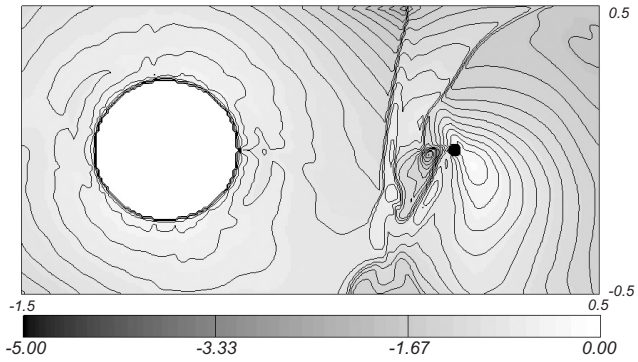

Fig. 7. Density contours in the orbital plane of the model E ($\gamma = 5/3$, $V_R = 0.68$). We observe very complicated shock patterns.

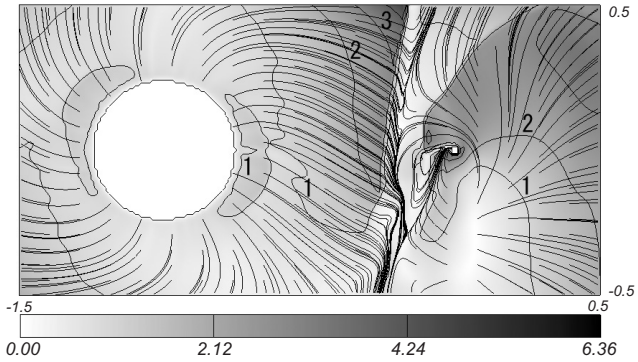

Fig. 8. Streamlines and Mach number contours in the orbital plane of the same model E as in Fig. 7.

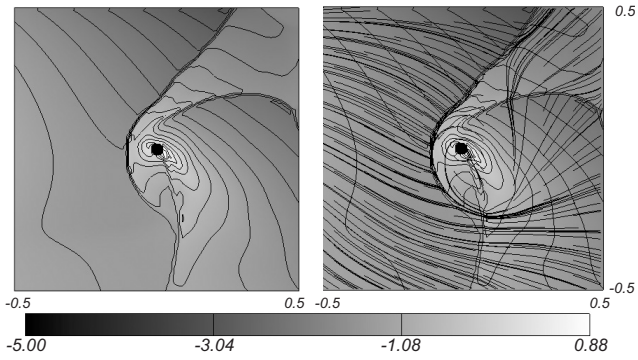

Fig. 9. Density contours and stream lines in the orbital plane of the model b ($\gamma = 1.01$, $V_R = 0.46$).

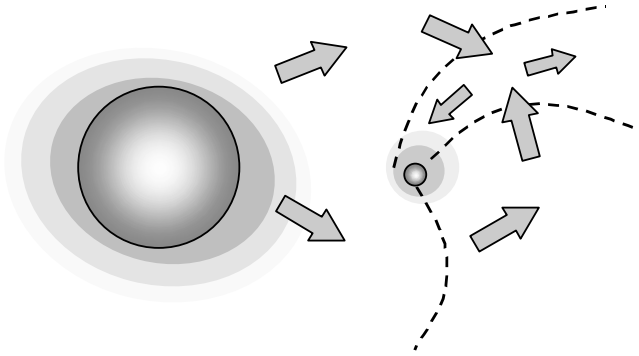

Fig. 10. A schematic diagram of an intermediate flow model E.

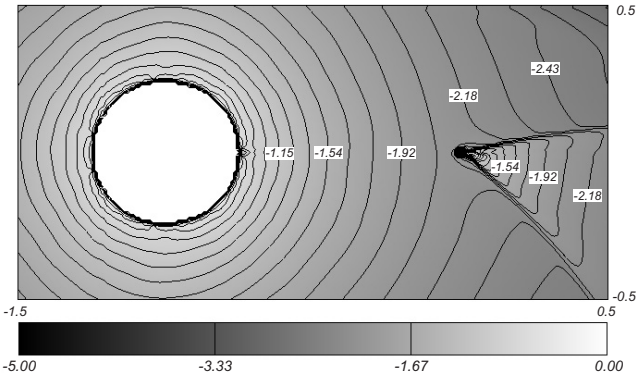

Fig. 11. Density contours in the orbital plane of a typical wind accretion flow model g ($\gamma = 1.01$, $V_R = 2.86$). We observe a conical bow shock attached to the accreting object, which is a typical feature of the wind accretion flow.

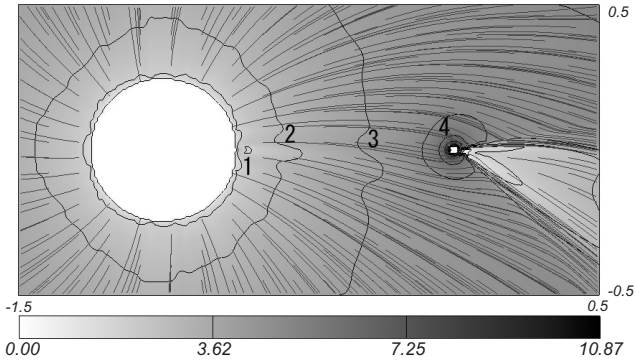

Fig. 12. Stream lines of the model g as in Fig. 11. Numbers are magnitude of normalized velocity.

3.4. Wind accretion flow

For the cases with $V_R > 0.7$, which are all the other models than stated above, the gas ejected from the mass-losing star is accelerated by thermal pressure. Almost all the gas escapes from the system and only a small part of the gas is accreted by the companion. We find a typical conical bow shock attached to the accreting object. Figures 11 and 12 show the density distribution, the streamlines and the magnitude of the velocity for model g ($\gamma = 1.01$, $V_R = 2.86$).

3.5. Calculations based on the nested grid

In order to test the effect of resolution near the mass accreting object, we calculate the flow using the nested grid described above. Figure 13 shows the density contours for model g′. If we compare the result of model g′ with that of model g, we can see a slight oscillation on the bow shock for model g′. Nevertheless, the essential features are unchanged except for the mass accretion efficiency.

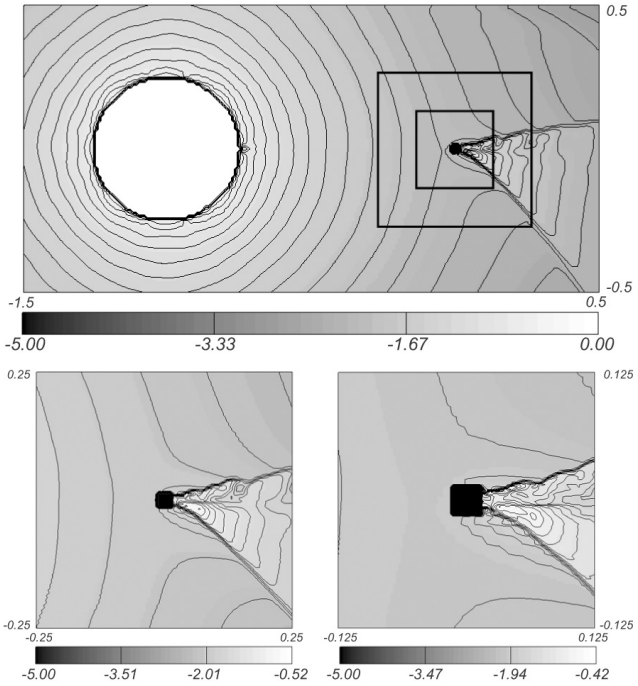

Fig. 13. Density contours of the model g′ ($\gamma = 1.01$, $V_{\rm R} = 2.85$) calculated on the nested grid. Two blow-ups close to the accreting star are shown. Compare the present figure with Fig. 11. We observe that the bow shock is slightly jaggy compared with Fig. 10. This is due to the reduced numerical viscosity.

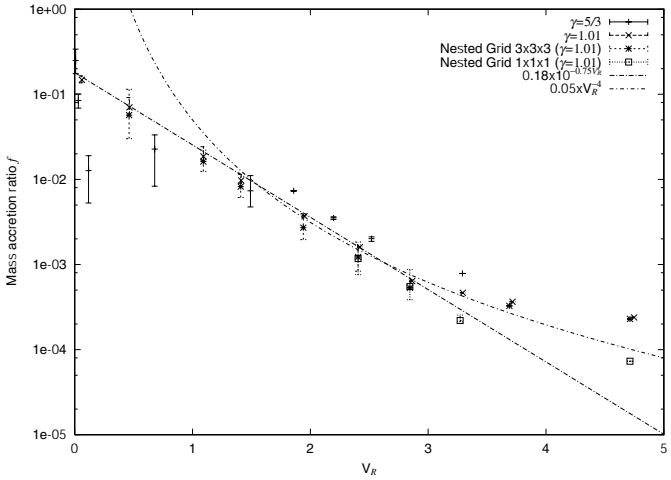

Fig. 14. Mass accretion ratio, defined by the ratio of the mass accretion rate to the mass loss rate, as a function of $V_{\rm R}$. The horizontal axis is $V_{\rm R}$ and the vertical one is the mass accretion ratio. The dash-dotted line is our empirical formula for the mass accretion ratio: $0.18 \times 10^{-0.75 V_{\rm R}}$, while the upper line is the fit valid for large $V_{\rm R}$.

3.6. Mass accretion ratio

We calculate the mass accretion ratio f, which is defined as the ratio of the mass accreting rate onto the companion, $\dot{M}_{\rm acc}$, to the mass loss rate from the mass losing star, $\dot{M}_{\rm loss}$. The mass accretion ratio as a function of $V_{\rm R}$ is shown in Fig. 14. The dash-dotted line is an empirical formula $f = 0.18 \times 10^{-0.75\ V_{\rm R}}$, which is valid in the range $V_{\rm R} < 2.5$.

In typical wind case we found that f is less than 1%, and decreases further with increasing $V_{\rm R}$ although it seems to saturate (but see below). In the intermediate flow regime, f is about a few% to 10%. For RLOF f is greater than 10% for $\gamma = 1.01$. If we use the above empirical formula to the limit of $V_{\rm R} = 0$, we have $f = 0.18$. Of course, this is not necessary true and $f = 1$ is also possible. Although a direct comparison is not possible, our values are in good agreement with the results obtained by TBJ96, Walder (1997), Mastrodemos & Morris (1998) or Dumm et al. (2000).

The curve of the calculated accretion ratio based on the coarse grid has a kink about $V_{\rm R} = 2.6$. This may be due to the fact that the size of the accreting cubic box may be comparable to or larger than the accretion radius. In order to see the effect, we reduced the size of the inner box. We found that the position of the kink is shifted towards larger $V_{\rm R}$, and the accretion ratio is reduced. This again is in agreement with the analysis done by TBJ96.

For high wind velocity, we expect the Hoyle-Lyttleton theory of wind accretion (Hoyle & Lyttleton 1939), that is the case where pressure force is neglected, to be applicable. If it is the case, then the mass accretion rate $\dot{M}_{\rm acc}$ must be proportional to the square of the mass accretion radius, $2GM/V_{\rm inf}^2$ – with $V_{\rm inf}$ being the wind velocity at infinity, and so we expect that $f \sim V_{\rm inf}^{-4}$. Assuming a spherical symmetric wind around the mass-losing component, we have

$$\dot{M}_{\rm wind} = 4\pi A^2 \rho_{\rm A} V_{\rm A}, \tag{1}$$

near the mass-accreting component. For a high wind velocity, we may expect that the accretion is determined by Hoyle & Lyttleton's formula, i.e.,

$$\dot{M}_{\rm acc} = \pi r_{\rm a}^2 \rho_{\rm A} V_{\rm A}, \tag{2}$$

and the accretion radius $r_{\rm a}$ is given by

$$r_{\rm a} = \frac{2GM_1}{V_{\rm A}^2}, \tag{3}$$

where $\rho_{\rm A}$ is the mass density, $V_{\rm A}$ is the wind velocity measured on the rotating flame, both at the mass accreting component, M_1 is the mass of the mass-accreting component. Therefore, the accretion ratio is calculated from

$$f = \frac{\dot{M}_{\rm acc}}{\dot{M}_{\rm wind}} \approx \left(\frac{V_{\rm A}}{A\Omega}\right)^{-4} \left(\frac{M_1}{M_1 + M_2}\right)^2. \tag{4}$$

Here, we use Kepler's relation of $A^3\Omega^2 = G(M_1 + M_2)$ and M_2 is the mass of the mass-losing component. For the present case of equal mass, the accretion ratio becomes

$$f = 0.25 \times \left(\frac{V_{\rm A}}{A\Omega}\right)^{-4}. \tag{5}$$

Note that we checked that the wind velocity does not change by a noticeable amount between the Roche lobe surface of the companion to the position of the primary. Hence, we can put $V_{\rm A} = V_{\rm R}$ in the above equation.

In Fig. 15 we show the accretion ratio as a function of $\log V_{\rm R}$. The upper line shows the simple Hoyle-Lyttleton formula as given by Eq. (5). The lower line shows another experimental formula $0.05\ V_{\rm R}^{-4}$, which agrees well with the calculated

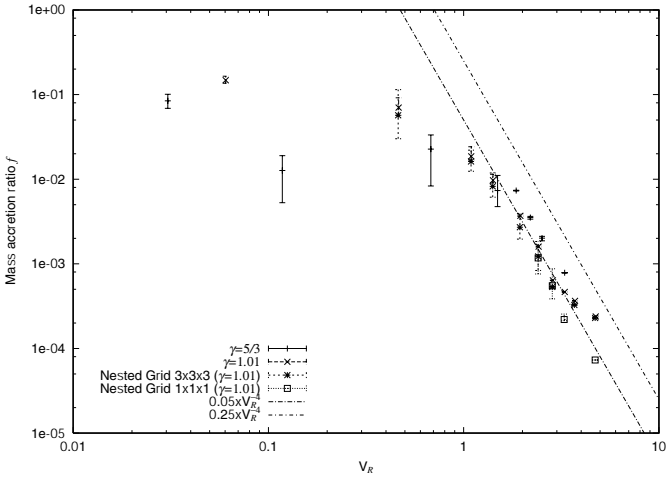

Fig. 15. Log–log plot of the Mass accretion ratio as a function of the wind velocity at the position of the Roche lobe. The upper line shows a simple Hoyle-Lyttleton formula as given by Eq. (5). The lower line shows another empirical formula $f = 5.0 \times 10^{-3}\ V_{\rm R}^{-4}$.

results for higher $V_{\rm R}$. It appears thus that the calculated mass accretion efficiency is about 20% of the predicted one. Such a comparison is however not fair for at least three reasons. First, because we take into account pressure, one should not use Hoyle-Lyttleton relation but rather the Bondi-Hoyle formula, and include the sound speed. Second, because our wind is thermally driven and we are in a binary system, it is not obvious at all to determine which wind velocity should be inserted in the equation. In the Hoyle-Lyttleton formalism, the velocity which is inserted is the upstream wind velocity at infinity. This is clearly meaningless in a close binary where the wind may not have reached its terminal velocity while close to the companion. Third, our wind is a diverging flow from the mass losing star, which contradicts the parallel upstream flow assumed in the Hoyle-Lyttleton or Bondi-Hoyle treatment. Therefore the use of the Hoyle-Lyttleton or Bondi-Hoyle formalism can be justified only qualitatively.

3.7. Time variation

We monitored the time variation of the mass accretion ratio. For intermediate flows the amplitude of time variation is about 30% for $\gamma = 1.01$ and it is about 70% for $\gamma = 5/3$. This trend that the amplitude of oscillation is larger for larger γ is applicable to other cases. For larger $V_{\rm R}$ cases the oscillation is negligible. In Fig. 14, the error bars show the amplitude of the oscillation of the mass accretion ratio. As was discussed above, the amplitude is larger for the finer grid because of the reduction of the numerical viscosity. By decreasing the size of the accreting box, we increase the range in $V_{\rm R}$ showing time variability. We Fourier analyzed the time sequence of mass accretion and did not find any typical frequency.

4. Conclusion

1. The flow pattern is classified by means of the normal speed of gas on the critical Roche surface, $V_{\rm R}$. For $V_{\rm R} < 0.4\ A\Omega$, we have a RLOF type flow, while for $V_{\rm R} > 0.7\ A\Omega$, wind accretion flows are realized. In the intermediate parameter range, $0.4\ A\Omega < V_{\rm R} < 0.7\ A\Omega$, we observe very complex flows.
2. We construct an empirical formula for the mass accretion ratio given by $f = 0.18 \times 10^{-0.75 V_{\rm R}/A\Omega}$, valid for low $V_{\rm R}$.
3. The calculated mass accretion ratio shows a kink at $V_{\rm R} \sim 2.6\ A\Omega$. By using the nested grid, we found that this is because the assumed size of the mass-accreting box is comparable to or larger than the accretion radius. By reducing the size of the mass-accreting box for the nested grid, the position of the kink is shifted to larger $V_{\rm R}$.
4. For larger $V_{\rm R}$ we obtain another empirical formula for the mass accretion ratio $f = 0.05(V_{\rm R}/A\Omega)^{-4}$.
5. For typical wind accretion flow, the results based on the coarse grid and those of the nested grid are essentially the same except the mass accretion ratio described above. For intermediate flow, the computed flow pattern depends on the resolution slightly. The amplitude of the oscillation of the flow increases with increased resolution because of reduced numerical viscosity.

Acknowledgements. We thank the anonymous referees for useful comments and remarks. Calculations were performed on the Origin 3800 at the information processing centre of Kobe University and on the NEC SX-5 at the Yukawa Institute of Kyoto University. K.O. was supported by the Research Fellowships of the Japan Society for Promotion of Science for Young Scientists. T.M. was supported by the grant in aid for scientific research of the Japan Society of Promotion of Science (13640241) and I.H. by (11640226). This work was supported by "The 21st Century COE Program of Origin and Evolution of Planetary Systems" in Ministry of Education, Culture, Sports, Science and Technology (MEXT).

References

Anupama, G. C., & Mikołajewska, J. 1999, A&A, 344, 177
Bennett, P. D., Harper, G. M., Brown, A., & Hummel, C. A. 1996, ApJ, 471, 454
Biermann, P. 1971, A&A, 10, 205
Blondin, J. M., Stevens, I. R., & Kallman, T. R. 1991, ApJ, 371, 684
Blondin, J. M., & Woo, J. W. 1995, ApJ, 445, 889
Bisikalo, D. V., Boyarchuk, A. A., Chechetkin, V. M., Kuznetsov, O. A., & Molteni, D. 1998, MNRAS, 300, 39
Boroson, B., Kallman, T., Blondin, J. M., & Owen, M. P. 2001, ApJ, 550, 919
Boffin, H. M. J., & Anzer, U. 1994, A&A, 284, 1026
Boffin, H. M. J., & Jorissen, A. 1988, A&A, 205, 155
Boffin, H. M. J., & Zàcs, L. 1994, A&A, 291, 811
Bondi, H., & Hoyle, F. 1944, MNRAS, 114, 195
Carquillat, J. M., Jorissen, A., Udry, S., & Ginestet, N. 1998, A&AS, 131, 49
Dumm, T., Folini, D., Nussbaumer, H., et al. 2000, A&A, 354, 1014
Foglizzo, T., & Ruffert, M. 1997, A&A, 320, 342
Foglizzo, T., & Ruffert, M. 1999, A&A, 347, 901
Fujiwara, H., Makita, M., Nagae, T., & Matsuda, T. 2001, Prog. Theor. Phys., 106, 729
Gawryszczak, A. J., Mikołajewska, J., & Różyczka, M. 2002, A&A, 385, 205
Hachisu, I., & Kato, M. 2001, ApJ, 558, 323

Hoyle, F., & Lyttleton, R. A. 1939, Proc. Camb. Phil. Soc., 35, 405
Kenyon, S. J., Livio, M., Mikołajewska, J., & Tout, C. A. 1993, ApJ, 407, 81
Makita, M., Miyawaki, K., & Matsuda, T. 2000, MNRAS, 316, 906
Mastrodemos, N., & Morris, M. 1998, ApJ, 497, 303
Matsuda, T., Inoue, M., & Sawada, K. 1987, MNRAS, 226, 785
Matsuda, T., Ishii, T., Sekino, N., et al. 1992, MNRAS, 255, 183
Matsuda, T., Makita, M., Fujiwara, H., et al. 2000, Ap&SS, 274, 259
Mikołajewska, J. 1997, in Physical Processes in Symbiotic Binaries and Related Systems, ed. J. Mikołajewska (Warsaw: Copernicus Foundation for Polish Astronomy), 3
Mürset, U., & Schmid, H. M. 1999, A&AS, 137, 473
Nussbaumer, H. 1991, Evolution in Astrophysics, Proc. IUE Symp., Toulouse, FR (Noordwijk: ESTEC)
Pogorelov, N. V., Ohsugi, Y., & Matsuda, T. 2000, MNRAS, 313, 198
Ruffert, M. 1996, A&A, 311, 817
Sawada, K., Hachisu, I., & Matsuda, T. 1984, MNRAS, 206, 673
Sawada, K., Matsuda, T., & Hachisu, I. 1986, MNRAS, 221, 679
Sion, E. M., & Ready, C. 1992, PASP, 104, 87
Sion, E. M., & Starrfield, S. G. 1994, ApJ, 421, 261
Sorensen, S.-A., Matsuda, T., & Sakurai, T. 1975, Ap&SS, 33, 465
Theuns, T., & Jorissen, A. 1993, MNRAS, 265, 946
Theuns, T., Boffin, H. M. J., & Jorissen, A. 1996, MNRAS, 280, 1264
Walder, R. 1997, in Accretion phenomena and related outflows, ed. D. T. Wichramasinghe, L. Ferrario, & G. V. Bicknell, IAU Colloq., 163, ASP Conf. Ser., 121, 822
Walder, R., & Folini, D. 2000, in Thermal and ionization Aspects of Flows from Hot Stars, ed. H. Lamers, & A. Sapar, ASP Conf. Ser., 204, 331